

We are IntechOpen, the world's leading publisher of Open Access books Built by scientists, for scientists

6,900

Open access books available

185,000

International authors and editors

200M

Downloads

Our authors are among the

154

Countries delivered to

TOP 1%

most cited scientists

12.2%

Contributors from top 500 universities



WEB OF SCIENCE™

Selection of our books indexed in the Book Citation Index
in Web of Science™ Core Collection (BKCI)

Interested in publishing with us?
Contact book.department@intechopen.com

Numbers displayed above are based on latest data collected.
For more information visit www.intechopen.com



Generation and Propagation of Frequency-Dispersive Tsunami

Claudia Cecioni and Giorgio Bellotti
*DSIC, University of Roma TRE
Italy*

1. Introduction

Tsunami are long water waves generated by sudden disturbances of the sea floor or sea water surface, which is usually caused by earthquakes, landslides or volcanic eruptions. Once triggered the tsunami can propagate over long distances, carrying destruction even on far coasts, hours after the impulsive generating event. The tragic consequences of the tsunami occurred the 26th December 2004 in the Indian Ocean, involved the scientific community to develop models able to reproduce the tsunami generation and their evolution, with the aim of building Tsunami Early Warning Systems.

A single model is not able to treat adequately the generation, propagation and inundation phase of tsunami scenarios, because it can not be at the same time accurate and computational efficient. The tsunami generation most of the times requires the solution of the full three dimensional equations of the hydrodynamics (Grilli et al., 2002; Liu et al., 2005), in order to accurately reproduce the complex sea floor motion and therefore the consequent wave field.

A mathematical problem which solves the three dimensional equations is especially needed when tsunami are generated by landslides or small submarine earthquakes. An other important feature which has to be taken into account when modelling the tsunami generation, are the nonlinear terms, which allow the reproduction of waves with a wave height of the same order of the water depth. The nonlinear equations have to be solved when the generating seismic event occurs close to the coast in shallow water, which represents the most dangerous threat for people and structures.

When the tsunami propagates far from the generating source it can reach high celerity, of the order of thousands of m/s. Tsunamis in deep water are long waves (wave length of the order of hundreds kilometres) with wave height of the order of one meter; therefore, if compared to the water depth (thousands of metres), can be considered small amplitude water waves. The tsunami propagation phase can therefore be accurately modelled using linear equations. When the wave propagation is to be studied over large geographical areas it appears natural to apply simplified equations in order to reduce the computational costs. These are the depth-integrated equations which reduce the full three-dimensional problem to a two-dimensional one, making the resulting model applicable over oceanic length scales. The most widely equations used are the long wave equations, named also Nonlinear Shallow Water Equations (NSWE). One weak point of the NSWE is that they are not able to reproduce properly the celerity at which each component of the wave field propagates.

According to those models one single celerity ($c = \sqrt{gh}$) governs all the components. However it has been demonstrated (Kulikov et al., 2005) that even tsunamis generated by large earthquakes are wave packets whose propagation can be relevantly influenced by the frequency dispersion. In the last years it has therefore become well accepted that the Boussinesq Type Equations (Peregrine, 1967; Lynett & Liu, 2005) are the most suitable tool for the computation of tsunamis. As far as the tsunami approaches the coastal areas the wave height increases and the nonlinear terms become again not negligible. In this phase tsunami can properly be reproduced using the shallow water approximation.

In this work we present a possible approach for the simulation of tsunami over large geographical areas. The model makes use of linear equations, because it considers the wave propagation in deep water, where the wave amplitude is much smaller than the water depth. The full frequency dispersion of the waves is reproduced, which in our opinion plays an important role in the tsunami propagation. A further point of interest is that, although developed to be used in the far field, the model seems to provide reasonable results also in the near field, and is able to reproduce the earthquake/landslide generation of the tsunamis. We believe the model to be useful for practical purposes because the computational procedure makes it suitable to support in real time a tsunami early warning system.

As it will be explained the model can be used to run a database of different tsunami scenario and then to elaborate in real time the tsunami waveform at some target points, by means of water level and seismic measurements while tsunami is occurring.

The model is based on the solution of the mild slope equation (MSE for short). The MSE has been originally developed by Berkhoff (1972) and it solves the wave field propagation at the undisturbed water free surface, by assuming a vertical structure of the wave motion as similar as that of the linear first order Stokes waves. The MSE in its original form is an elliptic equation which reproduces steady state situations for purely harmonic waves. Mathematically an elliptic equation defines a problem which is in general properly posed only if boundary conditions are specified, and it needs to be simultaneously solved over the whole computational domain. Copeland (1985) and Madsen & Larsen (1987) developed a pair of first-order equations, which constitutes a time dependent hyperbolic system, which is used to achieve the steady-state wave field induced by periodic waves. Kubo et al. (1992) and Kirby et al. (1992) studied the applicability of the time-dependent equations to random waves. However they concluded that only very narrow frequency wave spectra are properly reproduced by the hyperbolic versions of the MSE, since the equations coefficients are calculated using the frequency of the carrier wave. None of the above mentioned models seems able of dealing with broad spectrum wave field, such as that resulting for tsunamis. The novel approach followed here is inspired to the method used by Kirby et al. (1992), who separated the whole wave spectrum into several narrow bands and for each of these solved the time-dependent MSE. The proposed model solves the MSE in the frequency domain for all the wave frequencies, then it superimposes all the monochromatic solutions to obtain the broad banded spectrum wave field.

Although the model is originally derived for the wave propagation in the far field we also introduce a source term in the equations, which takes into account of the seafloor variation in time. We obtain the Mild Slope Equation with a generation term that describes the effect of the bottom movements on the surface waves. In order to incorporate the effects of the seafloor movements into depth integrated equation, it is often assumed that the bottom movements instantaneously transfer to the free water surface, which is treated as identical to the vertical component of the sea-floor deformation (Kajiura, 1970). This is especially valid

when the extension of the sea-floor rupture is very large in comparison to the water depth. However when the tsunami source is smaller, or of the same order of magnitude of the water depth (this is mostly the case of submerged landslide), the problem becomes more complicated. Tinti et al. (2006) proposed a filter function which attenuates the effects of the sea bottom movement in the water surface as the ratio between the water depth and the bottom movement extension becomes large. Starting from their work a slightly different filter function, applied to the MSE has been obtained (equation's derivation in the following section).

The chapter is structured as follows: section 2 describes the model equations; section 3 presents two set of experiments (physical and numerical) used to validate the model and it shows the application results on simulating landslide generated tsunami; section 4 describes the model abilities to work in a Tsunami Early Warning System and it shows an example of application to the South Tyrrhenian Sea (Italy, Mediterranean Sea). Finally in section 5 the conclusions are given. Part of the research presented in this chapter has been described in Cecioni & Bellotti (2010a, 2010b) and in Bellotti et al. (2008)

2. The proposed model

2.1 Model equation

The proposed model solves one elliptic MSE for each frequency of the wave spectrum, and then it applies the Inverse Fourier Transform to all the solutions in the frequency domain in order to recover the wave field time series. This procedure guarantees accurate reproduction of the frequency dispersion, since potentially all the components of the wave field are modelled using an appropriate elliptic equation.

In the following the MSE is derived, following the procedure of Svendsen (2005), which achieves the formulation of the time-dependented hyperbolic MSE. In the present equation's derivation, it is included a generation term by considering a time variation of the water depth function, in order to reproduce a bottom movement due to submarine earthquake or landslide. We start from the linear (small amplitude) water wave equations for an incompressible irrotational fluid on an uneven bottom

$$\nabla_h^2 \phi + \phi_{zz} = 0; \quad -h(x,y,t) < z < 0 \quad (1)$$

$$\phi_z + \frac{1}{g} \phi_{tt} = 0; \quad z = 0 \quad (2)$$

$$\phi_z + h_t + \nabla_h \phi \cdot \nabla_h h = 0; \quad z = -h(x,y,t) \quad (3)$$

where $\phi(x,y,z,t)$ is the velocity potential in the fluid, $h(x,y,t)$ is the water depth and g is the gravity acceleration, while ∇_h is the differential operator which means the divergence in the horizontal coordinates (x,y) . All these variables are real and scalar. Eq. (1) is the Laplace equation, Eq. (2) includes the linearized dynamic and kinematic boundary conditions at the free water surface, while Eq. (3) is the bottom boundary condition which reproduces the seafloor movements allowing h to vary in time. The solution of the given problem is assumed to be of the form

$$\phi(x,y,z,t) = \varphi(x,y,t)f(z) \quad (4)$$

where $\phi(x,y,t)$ is the velocity potential at the undisturbed free water surface $z = 0$, which can be complex and it includes the effects of reflected waves; $f(z)$ is a function that describes how the kinematic field varies along the water depth and can be chosen as that resulting from the linear wave theory valid for harmonic waves propagating in constant depth, which however still holds locally for uneven bottom, i.e.

$$f(z) = \frac{\cosh[k(h+z)]}{\cosh(kh)} \quad (5)$$

where k is the wave number, defined as $2\pi/L$ with L the wave length. In the cases of not constant depth, h and k vary with the horizontal coordinates, therefore $f = f(x,y,z)$. However if the mild slope assumption, $\frac{\nabla_h h}{kh} \ll 1$, is here introduced the variation of the function f with the horizontal coordinates can be neglected if compared with the vertical ones. From the assumption (4) it comes that

$$\phi_{zz} = k^2 \phi \frac{\cosh[k(h+z)]}{\cosh(kh)} = k^2 \phi \quad (6)$$

therefore the Laplace equation (1) can be written as

$$\nabla_h^2 \phi + k^2 \phi = 0 \quad (7)$$

The following considerations are made:

$$f(z) = 1; \quad z = 0 \quad (8)$$

$$f_z = k \tanh(kh) = \frac{\omega^2}{g}; \quad z = 0 \quad (9)$$

$$f_z = 0; \quad z = -h \quad (10)$$

In order to depth integrate the field equation (1), here it is made use of the Gauss's Theorem, which states for one dimensional domain

$$\int_a^b (\Phi_1 \nabla^2 \Phi_2 - \Phi_2 \nabla^2 \Phi_1) dx = [\Phi_1 \nabla \Phi_2 - \Phi_2 \nabla \Phi_1]_a^b \quad (11)$$

where Φ_1 and Φ_2 are arbitrary differentiable scalar functions. For the present purpose Eq. (11) is used with $x = z$, $\Phi_1 = f(z)$ and $\Phi_2 = \phi(x,y,z,t)$, therefore

$$\int_{-h}^0 \left(f \frac{\partial^2 \phi}{\partial z^2} - \phi \frac{\partial^2 f}{\partial z^2} \right) dz = \left[f \frac{\partial \phi}{\partial z} - \phi \frac{\partial f}{\partial z} \right]_0 - \left[f \frac{\partial \phi}{\partial z} - \phi \frac{\partial f}{\partial z} \right]_{-h} \quad (12)$$

Substituting the Laplace Eq. (1) in the first term at the left hand side (LHS), and the boundary conditions at $z = 0$ and $z = -h$ (Eqs. 2 and 3) and using Eqs. (9) and (10) in the right hand side (RHS) terms, then, after changing the sign, Eq. (12) becomes

$$\int_{-h}^0 (f \nabla_h^2 \phi + k^2 f \phi) dz = \frac{1}{g} \phi_{tt} + \phi \frac{\omega^2}{g} - [f h_t]_{-h} - [f \nabla_h h \cdot \nabla_h \phi]_{-h} \tag{13}$$

the LHS terms can be seen as the integration over the depth of the field equation. Considering that

$$\nabla_h \phi = \nabla_h (\phi f) = f \nabla_h \phi + \phi \nabla_h f \tag{14}$$

and

$$\nabla_h^2 \phi = f \nabla_h^2 \phi + 2 \nabla_h \phi \cdot \nabla_h f + \phi \nabla_h^2 f \tag{15}$$

using the expression (14) for the last term of the RHS and expression (15) for the first term of the LHS, Eq. (13) becomes

$$\begin{aligned} & \int_{-h}^0 (f^2 \nabla_h^2 \phi + 2 f \nabla_h f \cdot \nabla_h \phi + f \phi \nabla_h^2 f + k^2 f^2 \phi) dz = \\ & = \frac{1}{g} (\phi_{tt} + \omega^2 \phi) - \frac{1}{\cosh(kh)} h_t - [f \nabla_h h \cdot (f \nabla_h \phi + \phi \nabla_h f)]_{-h} \end{aligned} \tag{16}$$

Now incorporating the first two LHS terms of Eq. (16) it follows

$$\begin{aligned} & \int_{-h}^0 \nabla_h (f^2 \nabla_h \phi) dz + [\nabla_h h f^2 \cdot \nabla_h \phi]_{-h} + \phi k^2 \int_{-h}^0 f^2 dz = \\ & = \int_{-h}^0 \phi f \nabla_h^2 f dz - \phi \nabla_h h \cdot [f \nabla_h f]_{-h} + \frac{1}{g} (\phi_{tt} + \omega^2 \phi) - \frac{1}{\cosh(kh)} h_t \end{aligned} \tag{17}$$

Applying the Leibniz's rule for the first two LHS terms and knowing that

$$\int_{-h}^0 f^2 dz = \frac{cc_g}{g} \tag{18}$$

where c and c_g are respectively the phase and the group velocities, by multiplying Eq. (17) for g it results

$$\begin{aligned} & \nabla_h \cdot (cc_g \nabla_h \phi) + \phi k^2 cc_g - \phi_{tt} - \omega^2 \phi + h_t \frac{g}{\cosh(kh)} = \\ & -g \phi \left\{ \int_{-h}^0 f \nabla_h^2 f dz + \nabla_h h \cdot [f \nabla_h f]_{-h} \right\} \end{aligned} \tag{19}$$

Rigorously the identity of Eq. (18) is obtained for a single frequency of the wave spectrum, consequently Eq. (19) is valid for monochromatic waves, or can be seen as representative of narrow banded spectra sea state around a carrying frequency.

The RHS terms of Eq. (19) can be shown to be $O((\nabla_h h)^2, \nabla_h^2 h)$. Therefore, given the mild-slope assumption, $\nabla_h h \ll kh$, it can be argued that the RHS terms \ll LHS terms. Similarly, $\nabla_h^2 h \ll \nabla_h h$, which is a natural additional assumption because $\nabla_h^2 h = O(\nabla_h h)$ can only

occur over short distances without changing $O(\nabla_h h)$. This means that the RHS terms are \ll of all the others terms, we therefore get

$$\varphi_{tt} - \nabla_h \cdot (cc_g \nabla_h \varphi) + (\omega^2 - k^2 cc_g) \varphi = -h_{tt} \frac{g}{\cosh(kh)} \quad (20)$$

which is the **hyperbolic version of the MSE** in terms of fluid velocity potential and is usually referred to as the 'time-dependent mild-slope equation', allowing the simulation in the time-domain of the wave propagation. The so formulated MSE (20) solves the fluid velocity potential time series for a specified single wave frequency, which unambiguously determines the equation parameters, c , c_g , ω and k . The RHS term represents a source term, which takes into accounts the effects on the wave field of the bottom movement.

In terms of the free surface elevation η the MSE becomes (using the dynamic boundary condition at the free surface)

$$-\eta_{tt} + \nabla_h \cdot (cc_g \nabla_h \eta) - (\omega^2 - k^2 cc_g) \eta = -h_{tt} \frac{1}{\cosh(kh)} \quad (21)$$

Note that if the phase and group velocities are evaluated in the shallow water limit as $c = c_g = \sqrt{gh}$, then Eq. (21) reduces to the governing equation for forced long waves, with a filter function applied to the source term in order to attenuate its effect as bigger becomes kh . (Cecioni & Bellotti 2010b)

$$-\eta_{tt} + \nabla_h \cdot (gh \nabla_h \eta) = -h_{tt} \frac{1}{\cosh(kh)} \quad (22)$$

The **elliptic version of the MSE** can be obtained by taking the Fourier Transform of Eq. (21), then it comes

$$\nabla_h \cdot (cc_g \nabla_h N) + k^2 cc_g N = -fft(h_{tt}) \frac{1}{\cosh(kh)} \quad (23)$$

Where $N(x,y,\omega)$ is the Fourier Transform of $\eta(x,y,t)$, as $fft(h_{tt})$ is the Fourier Transform of h_{tt} . It can be noted that without allowing the bottom movement, i.e.: bottom boundary condition (3) without the term h_{tt} , the resulting equation would have been

$$\nabla_h \cdot (cc_g \nabla_h N) + k^2 cc_g N = 0 \quad (24)$$

which is properly the MSE as derived by Berkhoff (1972).

The RHS of Eq. (23) represents the source term of generating waves due to the bottom movement. It can be noted that this source term is formed by the water depth time variation and by a function which depends on the wave frequency, through the wave number. This function, $1/\cosh(kh)$, works as a low-pass frequency filter function between the movements of the bottom and those of the water free surface. In the proposed model, where the MSE is solved in the frequency domain, the inclusion of this frequency-dependend source term appears natural. Once Eq. (23) is solved, one for each frequency ω , with the appropriate boundary conditions, the result in the time domain can be achieved by taking the Inverse Fourier Transform of $N(x,y,\omega)$ to obtain $\eta(x,y,t)$. For details see Bellotti et al. (2008).

2.2 Boundary conditions

The solution of a elliptic equation requires the setting of all the boundaries of the numerical domain. The boundary conditions can allow the waves to be reflected on the boundary (reflection condition) or to freely exit the domain (radiation condition). The fully-reflection boundary condition can be expressed by imposing the fluid velocity in the direction orthogonal to the boundary to be zero. In the frequency domain the reflection condition at a boundary is expressed as follows

$$N_n = 0 \quad (25)$$

where n is the vector normal to the boundary.

The radiation boundary condition can be obtained by using a mathematical formulation that allows the waves propagating toward the open boundaries to freely exit the computational domain. This condition can be easily formulated for progressive outgoing waves

$$\eta_t + \frac{c}{\cos(\theta_n)} \eta_n = 0 \quad (26)$$

where θ_n is the angle the wave direction forms with the outgoing normal to the considered boundary. The Fourier Transform of equation (26) provides the radiation condition in the frequency domain

$$N_n + ik \cos(\theta_n) N = 0 \quad (27)$$

Please note that the equation (27) is nonlinear in the sense that θ_n is not known a priori and depends on the solution itself. Iterative techniques can therefore be applied or a reasonable estimate of this parameter can be used to solve the indeterminacy.

The wave generation in the numerical domain can be modeled with two different approaches: by means of a source term included in the field equation, as derived previously (Eq. 23), or by means of a wave-maker boundary condition. A wave-maker boundary condition can be seen as a wave paddle used in physical models (although here evanescent modes are not reproduced) and can be applied when the wave generation mechanism occurs close to a boundary of the numerical domain. The wave-maker boundary condition is conveniently formulated in terms of the velocity potential at $z = 0$ as follows

$$\phi_n = u^l, \quad z = 0 \quad (28)$$

where u^l is the velocity at $z = 0$ of the desired wave field orthogonal to the wave-maker boundary. In order to obtain a mathematical expression involving η and consequently N we make use of the dynamic boundary condition at the free surface which, if transformed in the frequency domain, results as follows

$$i\omega\Phi = -gN, \quad (29)$$

providing the usual relationship between Φ and N :

$$\Phi = -\frac{g}{i\omega} N \quad (30)$$

which allows rewriting of the wave-maker condition as

$$N_n = -\frac{i\omega}{g}U^I, \quad (31)$$

being U^I the Fourier Transform of the desired time series of velocity at $z = 0$. It is worth to remind that the proposed wave-maker condition is used to specify the fluid velocity at $z = 0$, and that the velocity field for $-h < z < 0$ is assumed to vary as the function f .

3. Validation against laboratory and numerical data

Here it is described the model validation, carried out by comparing the model results with those obtained from numerical and physical experiments, chosen as reference solution. The presented tests aim at reproducing tsunami generated by landslides. When a landslide occurs under the water in general it produces a sea floor perturbation which generates a complex three dimensional water flow in the proximity of the landslide itself. These perturbations are transferred to the water free surface depending on the water depth: if the landslide occurs in shallow water conditions, i.e. the landslide extension is larger compared to the water depth, then it can be assumed that at the water free surface occurs the same displacement of the sea bottom; this is not true when the landslide occurs in deep water conditions. In this case the column of water above the acts as a filter attenuating the bottom movement effects at the free surface.

The tests here presented will focus only on the reproduction of waves generated by landslides which propagate in deep water conditions.

In the following we present two sets of validation experiments: first the inclusion of the source term into the MSE (23) is analyzed through numerical experiments (see also Cecioni & Bellotti 2010a), which compare the proposed model solutions with the results of a three dimensional numerical solver, taken as reference. Then the results of a physical experiment are used to further validate the proposed model (see Cecioni & Bellotti 2010b). The physical model reproduces the landslide generated waves using a realistic model of the landslide, and a wave tank large enough to study the wave propagation in the far field. These experiments reproduce the particular case of a landslide falling at the flank of a conical island and they allow the analysis of the generated wave field close to the island and in the far propagation field.

3.1 Tsunami waves generation - numerical experiments (Cecioni & Bellotti 2010a)

Here a numerical experiment which reproduces tsunami generated by submerged landslide is described. The experiment has been carried out in order to validate the correct inclusion of the source term into the MSE, and to investigate on the ability of the proposed model, based on a depth integrated equation, to simulate the wave generation due to a sea bottom movement. The results of the proposed model are compared with those of a three dimensional one, which, as long as the linearized boundary conditions can be considered to be an acceptable approximation, can be regarded as the reference (i.e. the true) solutions. The three dimensional model solves the Laplace equation within the boundary conditions. It uses the same numerical scheme of the depth integrated model, thus the equations are solved in the frequency domain and are formulated as follows

$$\nabla_h^2 \Phi + \Phi_{zz} = 0 \quad (32)$$

$$\Phi_z - \frac{\omega^2}{g}\Phi = 0 \tag{33}$$

$$\Phi_n = f(t)(h_t) \tag{34}$$

$$\Phi_n + ik \cos(\theta_n)\Phi = 0 \tag{35}$$

where $\Phi(x,y,\omega)$ is the Fourier transform of $\phi(x,y,t)$. Eq. (32) is the Laplace equation, Eq. (33) is the free surface dynamic and kinematic boundary condition, Eq. (34) represents the moving bottom boundary condition and Eq. (35) is the radiation condition.

We have performed many computations, varying the water depth, the landslide length and kinematic. Here however, for the sake of brevity we limit to show results of one experiment, which can be considered representative of most of our simulations. In the sketch of Fig. 1 the numerical domain is represented, which is 10 m long and with a 1:3 slope; the landslide is a semi-ellipse, 4.21 m long and 0.1 m thick. The landslide suddenly starts to move after 10 s with a velocity of 1 m/s for 2 s and a total displacement of 2 m.

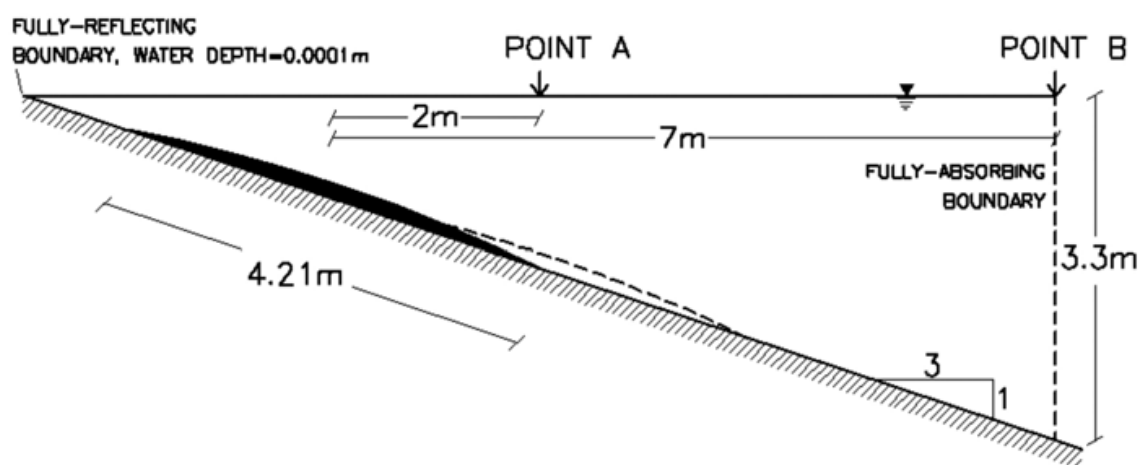


Fig. 1. Sketch of the computational domain

Numerical simulations were run with both the depth integrated model and the three dimensional one. The depth integrated model is applied in a one-dimensional domain, representative of the free water surface. At the left boundary ($x=0\text{ m}$) a reflecting boundary condition (Eq. 25) is imposed, by using a very small water depth (0.0001 m). At the right boundary, the water depth is equal to 3.3001 m and the waves are allowed to exit the domain, by applying the radiation condition (Eq. 27). The numerical simulations reproduce a time series of 100 s , using a Δt of 0.1 s . This results in a total of 1000 time steps, that in the frequency domain corresponds to the same number of angular frequencies, in the range between $2\pi \cdot 10^{-2}$ and $2\pi \cdot 10$. In the practice the MSE (23) is solved just for the frequencies $2\pi \cdot 10^{-2} \leq \omega \leq 2\pi \cdot 2$, where there is a significant content of wave energy. The higher frequency component reproduced has, for the considered water depth, a wave length of 4 m , thus the maximum distance between the computational nodes is 0.04 m , since a resolution of 10 nodes per wave length is required.

The three dimensional model is solved in a two dimensional domain which covers the fluid field represented in the sketch of Fig. 1. The imposed boundary conditions are: a fully

reflecting condition at the left boundary ($x=0$), where a small water depth is imposed as for the depth integrated model; a radiation condition along the right boundary ($x=10\text{ m}$); then at the free surface the Eq. (33) is applied, which combines the dynamic and kinematic conditions, while at the bottom boundary the wave generation condition (Eq. 34) is imposed. The same component of the wave spectrum of the depth integrated model are solved. The finite element grid is composed of triangular elements, with the maximum distances between the nodes of 0.04 m , as for the depth integrated model.

Fig. 2 shows the results of the numerical simulations in terms of surface elevation obtained with the depth integrated model (continuous black line) and the three dimensional one (dashed red line). The left and the right panels refer to the results at point A and B, where the water depth is about 1.6 m and 3.3 m respectively. The results of the two models appear to be in very good agreement both in the generation (left panel) and in the propagation areas (right panel).

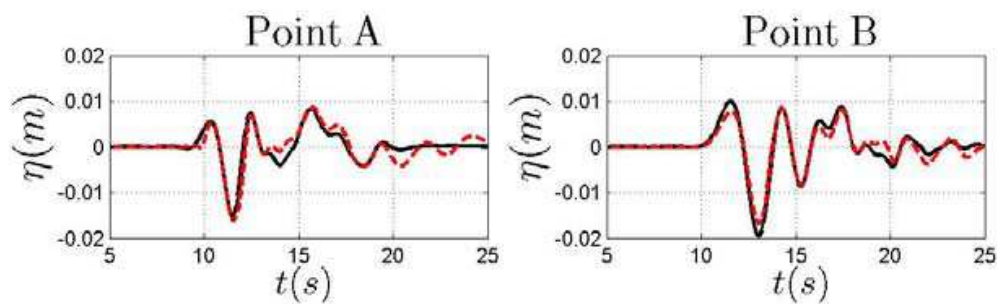


Fig. 2. Comparison of the free surface elevation obtained from the depth integrated model (continuous black line) and that obtained from the three dimensional model (dashed red line). The presented results are relative to the points A (left panel) and B (right panel) of Fig. 1.

These considerations can be supported by the analysis in the frequency domain. In Fig. 3 the left and right panels refer again to results picked up at the point A and B respectively. The thick black line represents the reference amplitude spectrum achieved with the three dimensional model, and the thin black line that obtained without using any filter in the depth integrated model, i.e.: the source term of the MSE is equal to the Fourier transform of the second derivative in time of the water depth function. The red line shows the amplitude spectrum obtained applying the MSE with the source term filtered by the wave frequency filter $1/\cosh(kh)$, Eq. (23).

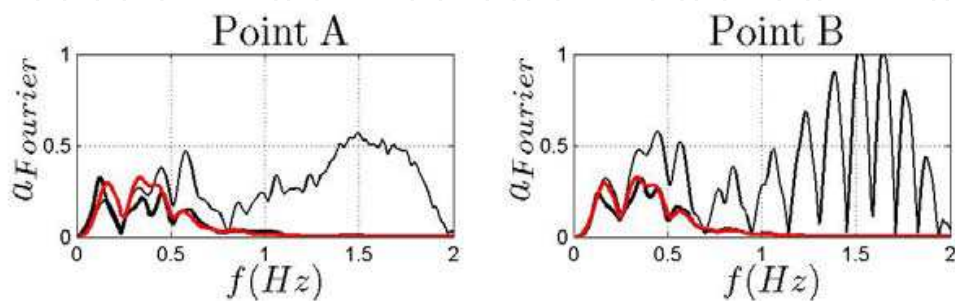


Fig. 3. Absolute values of the Fourier transform coefficients of the water surface elevations, computed with the three dimensional model (thick black line) and with the depth integrated model, without any filter function (thin black line), and computed with the proposed depth integrated model (red line).

It can be noted that from a physical point of view, the filter function has the effect of a low pass filter between the movements of the bottom and those of the free water surface. Translating the bottom deformation directly to the free surface introduces a large amount of spurious energy in the high frequency range, leading to unrealistic/wrong results.

3.2 Conical island experiments (Cecioni & Bellotti 2010b)

The results of physical experiments have been used in order to further validate the tsunami generation in the numerical model. The physical model was built in a large wave tank at the Research and Experimentation Laboratory for Coastal Defence (LIC) of the Technical University of Bari, Italy, in cooperation with the Environmental and Maritime Hydraulics Laboratory Umberto Messina (LIAM) of the University of L'Aquila, Italy. The laboratory experiments (Di Risio et al., 2009) simulate a landslide body falling on the flank of a conical island, built in order to approximately reproduce in scale 1:1000, the Stromboli island, south Tyrrhenian Sea, Italy (Tinti et al., 2006). The physical model consists in a wave tank, 30.00 m wide, 50.00 m long and 3.00 m deep; at the centre of the tank is placed a conical island, built using PVC sheets (thickness 0.01 m) and sustained by a steel frame, with a radius of 4.47 m at the tank bottom level. The slope of the flanks of the island is 1:3 (1 vertical, 3 horizontal, see the picture on the right of Fig. 4). Experiments have been carried out varying the water depth, and consequently the shoreline curvature radius, and by varying the initial distance of the landslide from the undisturbed shoreline. The landslide model is a rigid body, with the shape of an half of the ellipsoid described by the equation $x^2/a^2 + y^2/b^2 + z^2/c^2 = 1$, where $a = 0.2$ m, $b = 0.4$ m and $c = 0.05$ m, for a total volume $V = 0.0084$ m³. The landslide is constrained to slide down the inclined surface by means of rails. Traditional resistive gauges were employed to register the instantaneous vertical displacement of the free surface. All the signals have been acquired simultaneously at a frequency of 1000 Hz. The relative positions of all the gauges can be found in Fig. 4.

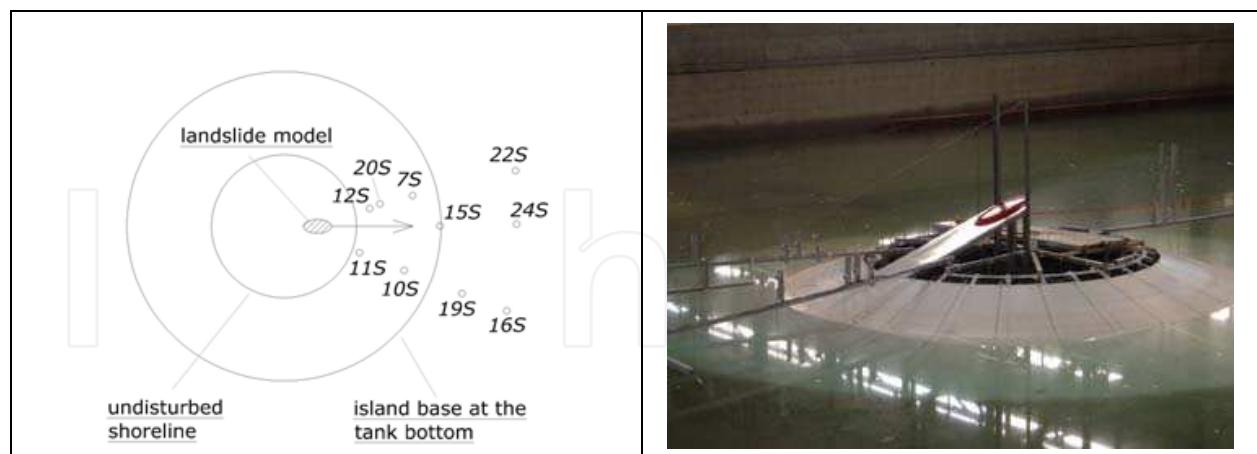


Fig. 4. Left: Layout of the sea-level gauges positions in the 3D tests at LIC. Right: Picture of the physical model.

The numerical computations have been carried out on a two-dimensional domain, sketched in Fig. 5. The numerical simulation here presented reproduces just one experimental case, defined by the off-shore constant water depth of 0.80 m, and the shoreline radius of 2.07 m, and characterized by an aerial landslide which falls from a distance of $\zeta = 0.30$ m from the undisturbed shoreline. In order to save computational costs, not all the wave tank was

numerically reproduced: the domain is circular around the island up to 8.00 m from the island centre; only half of the circular domain is reproduced given the symmetry of the problem (Fig. 5). At the internal circular border (the undisturbed shoreline) the reflection condition (25) is imposed. Along the external circular boundary the waves are allowed to freely exit the computational domain (Eq. 27). The landslide falls down in the direction of the right-bottom border, in Fig. 5. At that boundary the fully reflection condition is imposed in order to take into account the symmetric half of the domain which is not simulated.

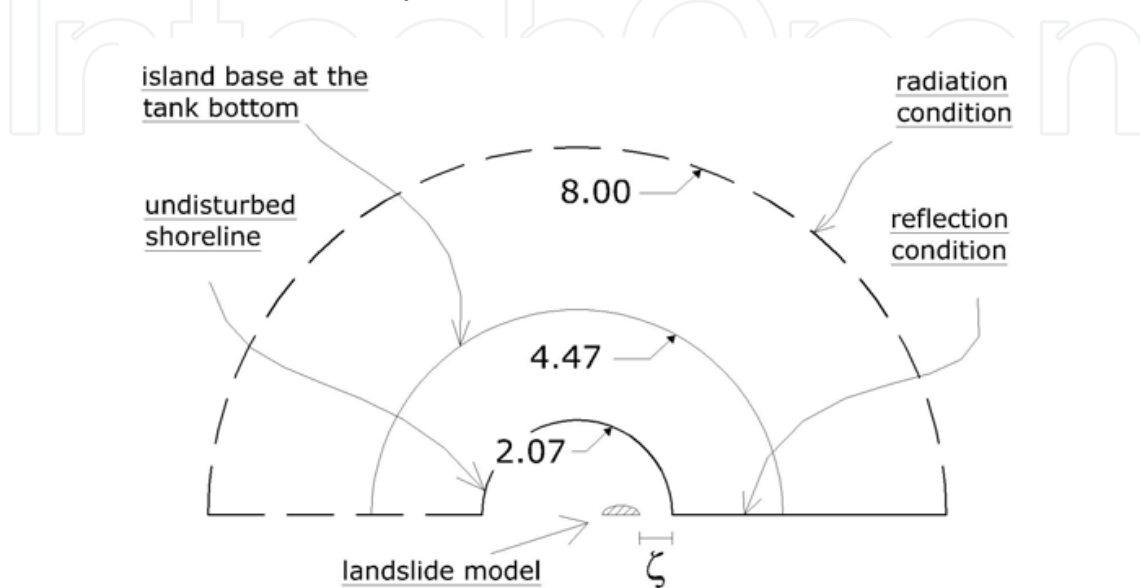


Fig. 5. Numerical domain of the depth integrated model. The numbers 2.07, 4.47 and 8.00 express the radii in meters of respectively the undisturbed shoreline, the island base at the tank bottom, and the external circular boundary.

The water depth function $h(x,y,t)$, which takes into account the sea floor motion, due to the landslide, is calculated by knowing the landslide shape and movement. The second derivative in time of the function, $h_{tt}(x,y,t)$, is carried out using a numerical approximation and its Fourier transform is applied, in order to insert it into the field Eq. (23). The numerical simulation has been carried out using triangular linear elements, whose maximum size is 0.05 m . Fig. 6 and 7 show the comparison between the laboratory measurement of the water surface elevation (red dashed lines) and the numerical simulations (solid black lines) at the gauges located as shown in Fig. 4.

As it can be seen from the figures, the model gives reliable results; this is evident especially for the gauges located in the off-shore area (refer to Fig. 4 for gauges position). The comparison shows that the model is not able to exactly reproduce the water level oscillations close to the shoreline, see the numerical results at gauges *S12* and *S11*. This behaviour can be explained because the linearity of the equation allows the reproduction of small amplitude landslide (or bottom movement), while in the entering phase the landslide is thick as the water depth. Moreover the numerical model equations are valid for submerged landslides, and no reproduction of the piston-like effect is made, which, which as seen in the laboratory experiment induces a deformation of the shoreline and it is responsible of the generation of waves propagating along the coast. Another point to be considered is that the numerical model does not reproduce any dissipation at the interface between water waves and the island.

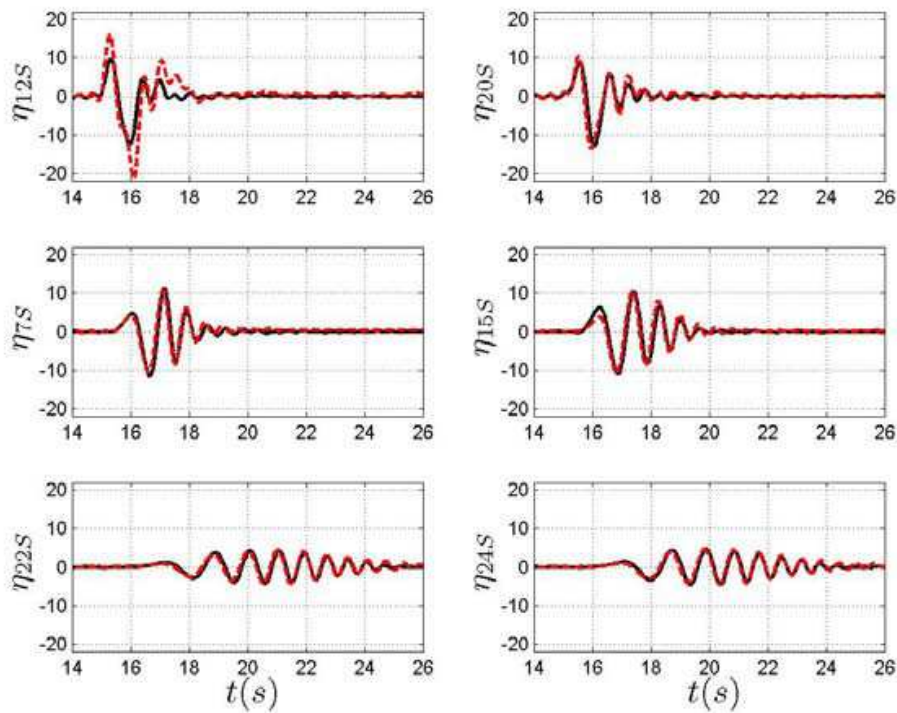


Fig. 6. Comparison of the free surface elevations (measures are in *mm*) at six gauges as measured in the physical model (red dashed line) and as obtained from the numerical model (black solid line).

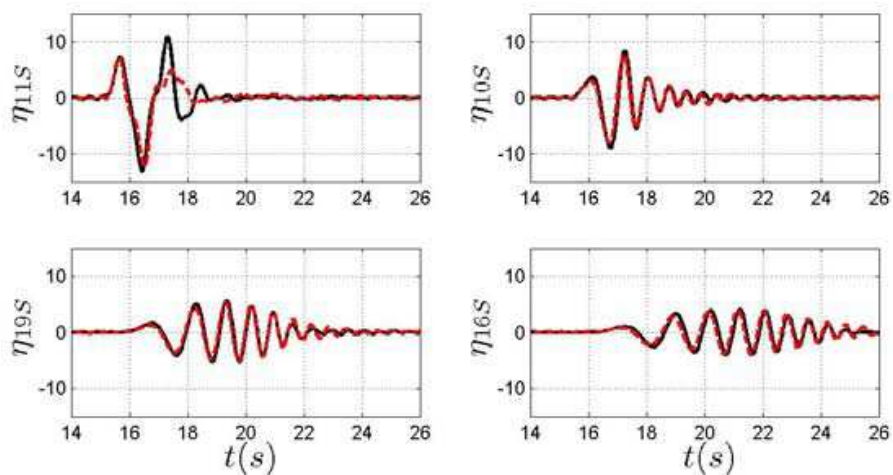


Fig. 7. Comparison of the free surface elevations (measures are in *mm*) at the other four gauges as measured in the physical model (red dashed line) and as obtained from the numerical model (black solid line).

4. Use of the model in a Tsunami early warning system

After the tragic event of December 2004, when an earthquake generated a tsunami that devastated the region of the Indian Ocean and killed about 250,000 people, the scientific community has been involved in the development of Tsunami Early Warning Systems

(TEWS for short). These systems should be triggered by seismic events, which are constantly monitored by worldwide efficient seismic networks. Once the occurrence of a submarine earthquake (or other tsunami sources, as landslides or volcanic eruptions) has been detected, rough estimates of the location of the epicentre and of the magnitude of the event are available after a short time. At that point a TEWS should decide if, given the properties of the earthquake, a tsunami alarm is to be spread. If positive, it should also be able to limit the alert to those people living at the coasts that are likely to be attacked by the waves.

It is also important that TEWS should be based on measurements of tsunami itself, in order to confirm or not that the earthquake has generated dangerous waves. It is therefore clear that, besides the earthquake and the water level measurements, a preliminary analysis is to be carried out in order to calculate the inundation level that any possible tsunami source is expected to induce along the surrounding coasts.

Many numerical models and different approaches can be used for performing the above mentioned analysis in order to build the database. Wei et al. (2003) proposed a model which solves the linear long wave equations. They have proposed an inverse method, which, thanks to the linearity of the equations, is able to infer seismic source parameters and tsunami wave form given the model simulations and water level data.

The presented model can be applied with the same scope to prepare a tsunami generation-propagation database, which results suitable in real time to forecast tsunami waveforms. The idea behind TEWS application, is to run preliminary computations without knowing the exact tsunami source, but assuming its location and here imposing a unitary wave generation term. The results of such preliminary computation are referred to as $N'(x,y,\omega)$. A second phase is applied in real time and it consists on estimating, by means of an inversion technique, the true solution. In view of the linearity of the problem the true solution in the frequency domain $N(x,y,\omega)$ can be obtained by multiplying N' for the Fourier Transform of the unknown source term, indicated as $S(\omega)$

$$N(x,y,\omega) = S(\omega) N'(x,y,\omega). \quad (36)$$

The model makes use of the sea level data (η_p) at one observation point P , in order to estimate the source term $S(\omega)$, by inverting Eq. (36) as follows

$$S(\omega) = N_p(\omega)/N'_p(\omega) \quad (37)$$

where N_p is the Fourier Transform of η_p and N'_p is the result of the unit source term computations at the same point P . If the records at more than one point are available, two alternative uses can be made of the data. On one hand it can be assumed that the source term is identical for all the generation areas/boundaries, and an optimization procedure can be used to find the value that best fits the data. On the other hand it can be assumed that each generation area/boundary has its own value of the source term and it is possible to write a linear system to be solved for these unknown source terms. Alternatively an over-determined system (the number of records available is greater than the number of source terms to be found) can be solved by means of an optimization procedure.

Here it is described a model application to Stromboli and the South Tyrrhenian sea. Stromboli is a volcano island in the deepwater Aeolian archipelago, Italy (Fig. 8). The NW flank of the island (named 'Sciara del fuoco') is unstable and frequently landslides occur at the coast, often related with volcanic activity. Some of these are able to generate tsunami waves which represent a real hazard for the surrounding islands and continental coast, as it

occurred on 30th of December 2002 (Tinti et al., 2005). Here we do not aim at exactly reproduce one specific tsunami event, but we build a numerical scenario just to show how the model can be applied in TEWS. Therefore, without having a tsunami water level registration at hand, we have assumed to measure a tsunami event characterized by a N-wave with period of 1 min and height of 30 m in deep water in front of Stromboli. This wave form is chosen after careful evaluation of the conclusions of Tinti et al. (2006), who analyzed the December 2002 tsunami event .

Fig. 8 shows the computational domain used, which encloses the islands of Stromboli, Panarea and Basiluzzo. A wave-maker condition, as that expressed by equation (31), is imposed at the boundary of the Stromboli island along the coast of the ‘Sciara del fuoco’. For the preliminary computation at this boundary a unit value is assigned at the free surface fluid velocity U^i . The boundaries of the islands are modeled as impermeable and fully-reflecting using Eq. (25), while in the circular outer boundary a fully-absorbing condition is imposed to allow the outgoing waves radiation (27). The results of the preliminary computation are saved at four points of interest: point 1 is just at the wave-maker boundary; point 2 is South-West of the generation area, in proximity of the Ginostra village, along the coast; point 3 is about at the South corner of the island, in proximity of Punta Lena; finally the results in proximity of Basiluzzo, 14 km away from the island are presented at point 4.

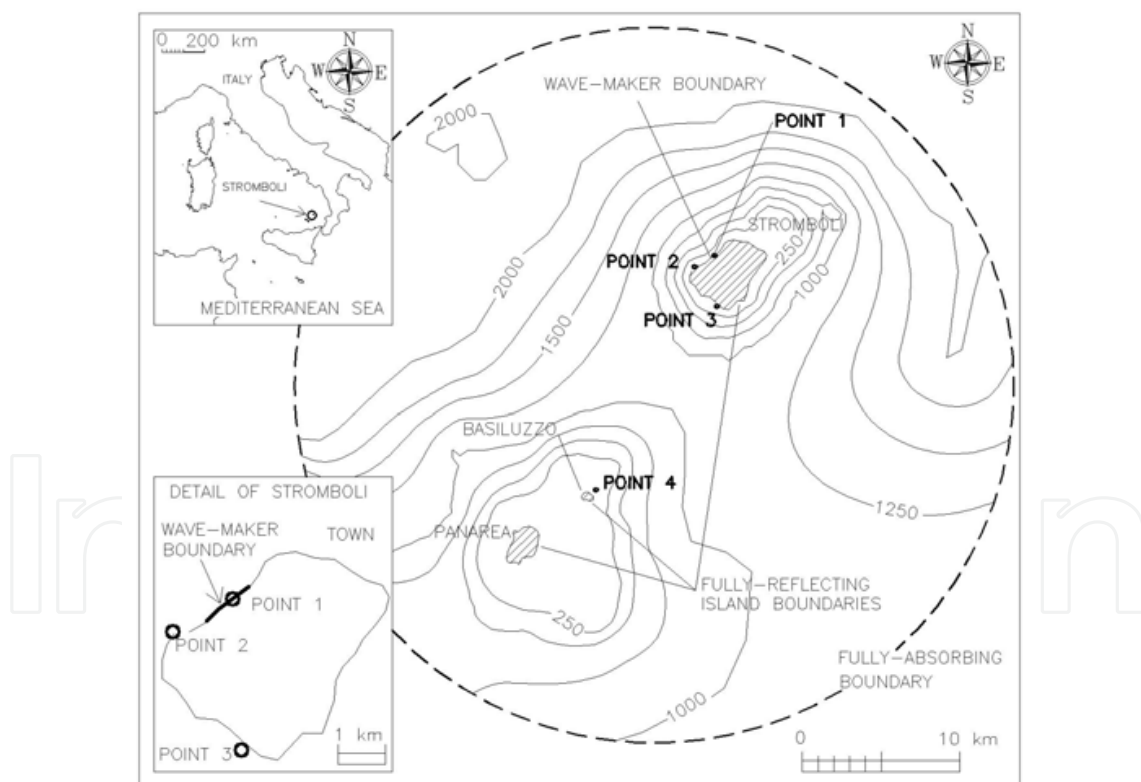


Fig. 8. Computational domain of the Stromboli-Panarea tsunami simulations.

Once the preliminary computation is carried out, we suppose that a landslide falls at ‘Sciara del Fuoco’ and it produces a tsunami which induces at point 1 a sea level elevation exactly as the N-wave. Thanks to the linearity of the model equations it is possible to apply Eq. (37) at the point 1 and therefore estimate the source term which has produced the N-wave at

point 1. In Fig. 9 we can see the results in term of sea level elevation at the four points. It can be noted that as the distance from the 'Sciara del Fuoco' source grows, the height of the first positive wave reduces, and it appears other waves following. It can be noted at the other points 3 and 4, that the first incoming wave is not the highest. In particular at the point 4, in front of Basiluzzo Island (the most distant point from the generation area considered here) the first wave arrives for both models after about 240 s, which is consistent with the shallow water wave celerity in a constant water depth equal to the mean water depth between Stromboli and Basiluzzo (about 600 m).

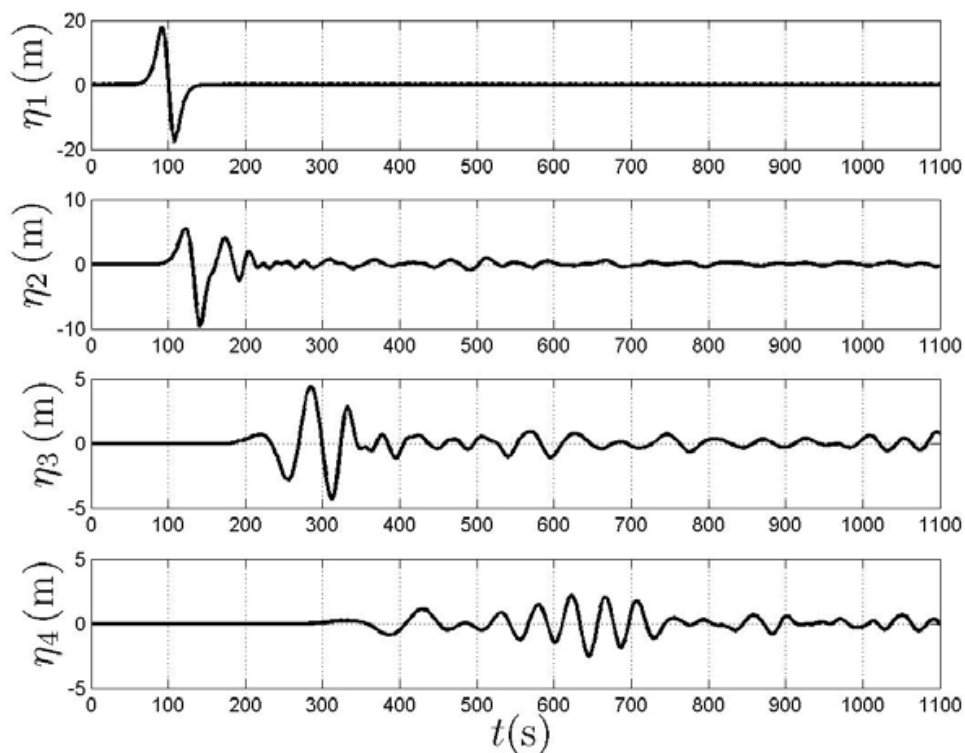


Fig. 9. Numerical results of the Stromboli-Panarea tsunami computation. Time series of the water free surface elevation as measured at point 1 and as forecasted at the other points by the model.

In Fig. 10 it is shown how the model works even with truncated input time series, in order to show which is the tsunami prediction at the target point (point 4) as the tsunami is being measured at the observation point (point 1). Several computations have been performed, assuming that the input time series is available up to a given time (t_{known}):

$$\eta_{input}(t) = \eta_1(t), t \leq t_{known}$$

$$\eta_{input}(t) = 0, t > t_{known}$$

The results depend therefore on the value of t_{known} , as longer is the duration of the tsunami registration available at point 1, as better is the tsunami prediction at point 4. However it is clear that is unrealistic, given the limited time available for spreading the warning, to wait until the tsunamis has been completely measured. Few sample results are reported in Fig. 10, where the time series at the point 4 (named Panarea) are presented for $t_{known} = 484, 496, 512$ and 556 s.

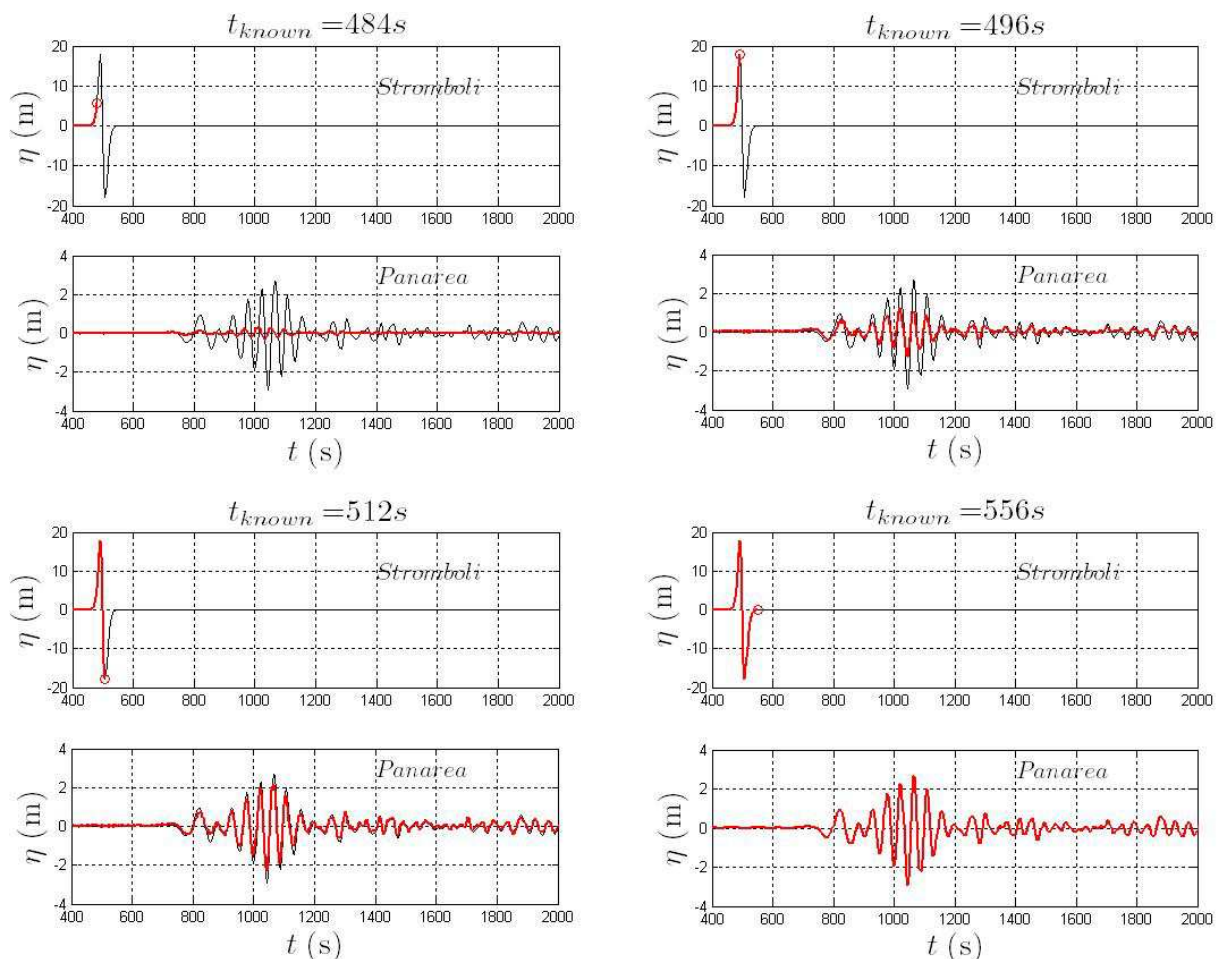


Fig. 10. Example of application of the model using truncated input time series. In each subplot the upper panel refers to the mareogram at point 1 of Fig. 8 (Stromboli) and the lower panel refers to point 4 of Fig. 8 (Panarea). The red line represents the truncated input data registered at Stromboli and predicted at Panarea, while the black lines refer to the whole mareogram registration.

On the upper panel of each subplot the input time series (η at point 1, in front of Stromboli) is represented using a thick red line, while on the lower panels it is shown the predicted η at point 4, in front of Panarea island. It is interesting to note that the use of a truncated input time series introduces very high frequency components, that are revealed by spurious short waves in the results. For $t_{known} = 496$ s the crest of the first (highest) wave is used in the input time series and the prediction at Panarea appears to be already comparable to the final one. For $t_{known} = 512$ s, 3/4 of the first wave in front of Stromboli is used with very good results at Panarea. Then the results tend to those that would be obtained using the whole time series. The most important parameter predicted by the model is certainly the maximum elevation at the point 4 (Panarea), referred to as η_{max} . As the t_{known} increases the prediction tends to the final one, as shown in the Fig. 11. The vertical line in the figure represents the time at which the crest of the first wave is measured at point 1 (around $t = 500$ s). The horizontal line indicates the final value of η_{max} . It is interesting to note that due to spurious high frequency components, induced by the truncation of the input time series, for some values of the t_{known} , η_{max} may be larger than the final one. However it can be concluded that the

model is able to dynamically provide estimates of the desired parameter without suffering of instabilities. It is certainly desirable to carry out further research in the future in order to better understand if this good behavior of the model can be considered to apply under more general conditions.

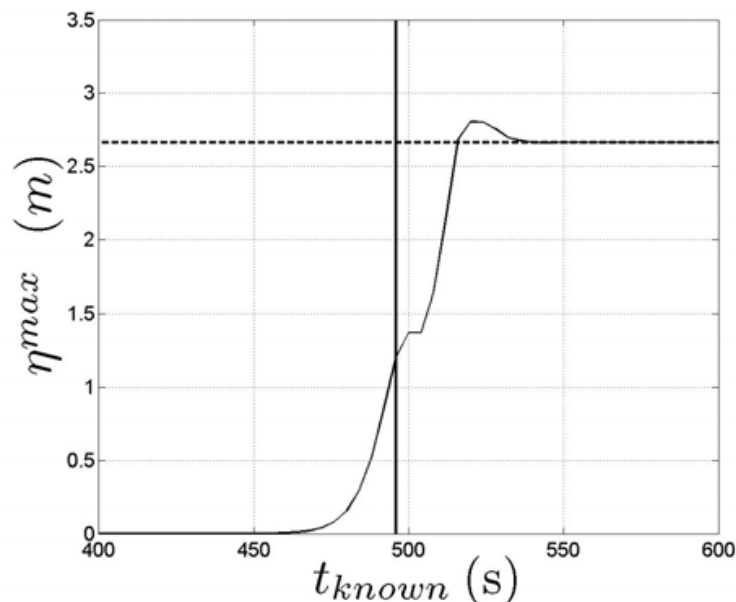


Fig. 11. Example of application of the model using truncated input time series; maximum surface elevation in front of Panarea island (point 4 of Fig. 8) as the time series at Stromboli (point 1) becomes available.

5. Conclusion

In this chapter we have presented a numerical model able to reproduce small amplitude transient waves. The model is based on linear equations, therefore it can properly reproduce waves generated and propagating in deep water. The wave generation is reproduced by forcing the mild slope equation, in order to include the effect at the free water surface due to sea floor movements. The comparison with the results obtained from a completely three dimensional laboratory experiments have proven the ability of the model to simulate wave generation and propagation.

An important feature of the presented model is that it considers the full frequency dispersion of waves, and in this sense is similar to the Boussinesq equations, when applied to small-amplitude waves. It has been demonstrated that tsunamis, although considered long wave, propagate with a celerity which is strongly influenced by the frequency. The ability of predicting with good accuracy the celerity is of the utmost importance when estimating the arrival time of the tsunamis. However the frequency dispersion has also a further very important effect on the transient waves: it induces a decrease of the wave height, especially for the first waves of a wave packet. This behaviour appears very clear in the TEWS application at Stromboli presented in this chapter, where the comparison of the results of the present model with those obtained using the linear shallow water equations has allowed to highlight this effect. It has resulted that only due to this, the wave height predicted by the LSWE can overestimate the actual height, for the experiments presented

here also of a factor of 2. On the one hand it could be stated that the wave conditions predicted by the SWE are more severe than the real ones, so that safety is guaranteed. However, on the other hand, predicting tsunamis much more severe than the true ones in the context of a tsunami early warning system may lead to false alarms, which induce people not to trust the system, with possible catastrophic consequences.

6. Acknowledgements

This work was carried out under the research projects PRIN 2007 (“Development and validation of hydraulic and geologic tools for supporting a Tsunami Early Warning System. Implementation to the Stromboli Eolie-landslide case.”) and FIRB 2008 (“Design, construction and operation of the SMO - Submarine Multidisciplinary Observatory-experiment”), both funded by the Italian Ministry for University and Scientific Research (MIUR).

7. References

- Bellotti, G., Cecioni, C. & De Girolamo, P. (2008). Simulation of small amplitude frequency-dispersive transient waves by means of the mild slope equation. *Coastal Engineering*, 55 (6), 447-458.
- Berkhoff, J.C.W. (1972). Computation of combined refraction-diffraction. *Proceedings of the 13th International Conference on Coastal Engineering ASCE*, Vancouver, Canada.
- Cecioni, C. & Bellotti, G. (2010a). Modelling tsunami generated by submerged landslides using depth-integrated equations. *Applied Ocean Research*, 32(3), 343-350.
- Cecioni, C. & Bellotti, G. (2010b). Inclusion of tsunamis generation into a depth integrated wave propagation model. *Natural Hazard and Earth System Sciences*, 10, 2259-2268
- Copeland, G.J.M. (1985). A practical alternative to the mild-slope wave equation. *Coastal Engineering*, 9, 125-149.
- Di Risio, M., De Girolamo, P., Bellotti, G., Panizzo, A., Aristodemo, F., Molfetta, M.G. & Petrillo, A.F. (2009). Landslide generated tsunamis runup at the coast of a conical island: New physical model experiments. *Journal of Geophysical Research*, 114.
- Grilli, S. T.; Volgemann, S. & Watts, P. (2002). Development of a 3D numerical wave tank for modelling tsunami generation by underwater landslides. *Engineering Analysis with Boundary Elements*, 26, 301-313.
- Kajiura, K. (1970). Tsunami source, energy and the directivity of wave radiation. *Bulletin Earthquake Res. Inst., Univ. Tokyo*, 48, 835-869.
- Kirby, J.T., Lee, C. & Rasmussen, C. (1992). Time-Dependent Solutions of the Mild-Slope Wave Equation. *Proceedings of the 23th International Conference on Coastal Engineering -ASCE*, Venice, Italy, 391-404. By Billy L. Edge, (editor), New York, 0-87262-933-3.
- Kubo, Y., Kotake, Y., Isobe, M. & Watanabe, A. (1992). Time-Dependent Mild Slope Equation for Random Waves. *Proceedings of the twenty-third International Conference on Coastal Engineering - ASCE*, Venice, Italy, 419-431. By Billy L. Edge, (editor), New York, 0-87262-933-3.
- Kulikov, E.A.; Medvedev, P.P. & Lappo, S.S. (2005). Satellite recording of the Indian ocean tsunami on December 26, 2004. *Doklady Earth Sciences*, 401A, 3, (2005), 444-448.

- Liu, P. L.-F.; Wu, T.-R.; Raichlen, F.; Synolakis, C. E. & Borrero, J. C. (2005). Runup and rundown generated by three-dimensional sliding masses. *Journal of fluid Mechanics*, 536, 107-144.
- Lynett, P. & Liu, P.L.-F. (2002). A numerical study of submarine-landslide-generated waves and run-up. *Proc. Royal Society London*, 458, 2885-2910.
- Madsen, P.A., Larsen, J., 1987. An efficient finite-difference approach to the mild-slope equation. *Coastal Engineering*, 11(4), 329-351.
- Peregrine, D.H. (1967). Long waves on a beach. *Journal of Fluid Mechanics*, 27, 815-827.
- Svendsen, Ib.A. (2005). Introduction to nearshore hydrodynamics. *Advanced Series on ocean Engineering*, 24, World Scientific, ISBN 981-256-204-4.
- Tinti, S., Pagnoni, G. & Zaniboni, F. (2006). The landslide and tsunamis of the 30th of December 2002 in Stromboli analyzed through numerical simulations. *Bulletin of Volcanology*, 68 (5), 462-479.
- Tinti, S., Manucci, G., Pagnoni, G., Armigliato, A. & Zaniboni, F. (2005). The 30 December 2002 landslide-induced tsunamis in Stromboli: sequence of the events reconstructed from the eyewitness accounts. *Natural Hazard and Earth System Sciences*, 5, 763-775.
- Wei, Y., Cheung, K.F., Curtis, G.D. & McCreery, C.S. (2003). Inverse algorithm for tsunami forecasts. *Journal of Waterway, port, Coastal and Ocean Engineering*, ASCE, 129(2), 60-69.

IntechOpen



The Tsunami Threat - Research and Technology

Edited by Nils-Axel MÅrner

ISBN 978-953-307-552-5

Hard cover, 714 pages

Publisher InTech

Published online 29, January, 2011

Published in print edition January, 2011

Submarine earthquakes, submarine slides and impacts may set large water volumes in motion characterized by very long wavelengths and a very high speed of lateral displacement, when reaching shallower water the wave breaks in over land - often with disastrous effects. This natural phenomenon is known as a tsunami event. By December 26, 2004, an event in the Indian Ocean, this word suddenly became known to the public. The effects were indeed disastrous and 227,898 people were killed. Tsunami events are a natural part of the Earth's geophysical system. There have been numerous events in the past and they will continue to be a threat to humanity; even more so today, when the coastal zone is occupied by so much more human activity and many more people. Therefore, tsunamis pose a very serious threat to humanity. The only way for us to face this threat is by increased knowledge so that we can meet future events by efficient warning systems and aid organizations. This book offers extensive and new information on tsunamis; their origin, history, effects, monitoring, hazards assessment and proposed handling with respect to precaution. Only through knowledge do we know how to behave in a wise manner. This book should be a well of tsunami knowledge for a long time, we hope.

How to reference

In order to correctly reference this scholarly work, feel free to copy and paste the following:

Claudia Cecioni and Giorgio Bellotti (2011). Generation and Propagation of Frequency-Dispersive Tsunamis, The Tsunami Threat - Research and Technology, Nils-Axel MÅrner (Ed.), ISBN: 978-953-307-552-5, InTech, Available from: <http://www.intechopen.com/books/the-tsunami-threat-research-and-technology/generation-and-propagation-of-frequency-dispersive-tsunamis>

INTECH
open science | open minds

InTech Europe

University Campus STeP Ri
Slavka Krautzeka 83/A
51000 Rijeka, Croatia
Phone: +385 (51) 770 447
Fax: +385 (51) 686 166
www.intechopen.com

InTech China

Unit 405, Office Block, Hotel Equatorial Shanghai
No.65, Yan An Road (West), Shanghai, 200040, China
中国上海市延安西路65号上海国际贵都大饭店办公楼405单元
Phone: +86-21-62489820
Fax: +86-21-62489821

© 2011 The Author(s). Licensee IntechOpen. This chapter is distributed under the terms of the [Creative Commons Attribution-NonCommercial-ShareAlike-3.0 License](#), which permits use, distribution and reproduction for non-commercial purposes, provided the original is properly cited and derivative works building on this content are distributed under the same license.

IntechOpen

IntechOpen